Journal of Solid State Chemistry **156,** 370–378 (2001)
doi:10.1006/jssc.2000.9008, available online at http://www.idealibrary.com on IDEAL®

Synthesis and Structure of Novel Cr^{V}–Cr^{VI} Mixed Valence Compounds, $Nd_{1-x}Ca_xCrO_4$ ($x = 0.02$–0.20)

Y. Aoki and H. Konno

Division of Materials Science and Engineering, Graduate School of Engineering, Hokkaido University, Sapporo, 060-8628 Japan

Received July 11, 2000; in revised form September 27, 2000; accepted October 13, 2000; published online December 21, 2000

Single phase $Nd_{1-x}Ca_xCrO_4$ ($x = 0$–0.20) oxides were synthesized by the pyrolysis of precursors prepared from Nd^{III}–Ca^{II}–Cr^{VI} mixed solutions. $Nd_{1-x}Ca_xCrO_4$ having $x \geq 0.25$ was not obtained as a single phase. All $Nd_{1-x}Ca_xCrO_4$ were zircon type (tetragonal, $I4_1/amd$), and the composition was almost stoichiometric without any essential defects, which was determined by chemical analyses. The lattice constants and atomic positions was refined by the X-ray Rietveld method. The calculated densities of $Nd_{1-x}Ca_xCrO_4$ ($x = 0$–0.20) were in good agreement with the ones measured by the picnometry. XPS and Raman spectra indicated that $Nd_{1-x}Ca_xCrO_4$ ($x = 0.02$–0.20) are mixed valence oxides containing two types of tetrahedra, $Cr^{V}O_4^{3-}$ and $Cr^{VI}O_4^{2-}$, having D_{2d} symmetry in the structure, and this compensates the decrease of positive charges introduced by Ca^{II} ions. Though two types of tetrahedra were not distinguishable by XRD, lattice constants a and c decreased almost linearly with x. The values for $x = 0.02$–0.20, however, were not on the line expected by Vegard's law between $NdCrO_4$ and $CaCrO_4$ but larger. The calculated O–Cr–O bond angles, however, did not change monotonously as lattice constants and other crystallographic parameters such as Cr–O bond length did, indicating that CrO_4 tetrahedra in $Nd_{1-x}Ca_xCrO_4$ ($x = 0.02$–0.20) are more elongated than in $NdCrO_4$ and $CaCrO_4$. It was deduced that the limit of x (about 0.25) may be determined by the difference in geometry between $Cr^{IV}O_4^{2-}$ and $Cr^{V}O_4^{3-}$ tetrahedra. © 2001 Academic Press

Key Words: **pentavalent chromium ion; Cr^{V}–Cr^{VI} mixed valence compound; Raman spectroscopy; CrO_4^{3-} tetrahedron; X-ray Rietveld structure refinement; X-ray photoelectron spectroscopy; zircon type oxide; Elongation of tetrahedron.**

INTRODUCTION

Unusual valence state cations, such as Ti^{III}, Cr^{IV}, Cr^{V}, Mn^{V}, Fe^{VI}, and so on, doped in various oxides have been studied because of their remarkable luminescent properties and application to the tunable lasers of near infrared (1–7). Not the doped Cr^{V} but pentavalent chromium oxides have been studied since early times. The tetrahedrally coordinated $Cr^{V}O_4^{3-}$ ion is rather unstable but the compounds with rare earth elements (Ln) are exceptionally stable in an ambient atmosphere. Therefore, many studies are reported on the $LnCrO_4$-type compounds (8–17). Because $LnCrO_4$ consists of two kinds of magnetic ions, Ln^{III} and Cr^{V}, some studies have been carried out on the complex magnetic behaviour due to the interaction between them (12, 13, 15–17). In the case of Ln = Nd–Lu, $LnCrO_4$ has a zircon-type structure (tetragonal, $I4_1/amd$) (9, 10, 14). The zircon-type structure $NdCrO_4$ is built from chains of alternating edge-sharing CrO_4^{3-} tetrahedra and NdO_8 bisdisphenoids. This CrO_4^{3-} tetrahedron is slightly elongated, because the O–O edges shared with NdO_8 are shorter than the length of the unshared tetrahedral edges. However, the detailed structures, such as accurate atomic positions, interatomic distances, and so on, had not been reported until our previous paper (18). We have reported that $NdCrO_4$ can be synthesized as a single phase by pyrolysis of the precursor prepared from equimolar mixed solutions of Nd^{III} and Cr^{VI} and have determined the detailed structure by X-ray Rietveld refinement (18).

In the present work, we attempted to synthesize the mixed valence compounds of Nd^{III}, Cr^{V}, and Cr^{VI} by doping Ca^{II} into $NdCrO_4$, since $CaCr^{VI}O_4$ has a zircon-type structure (19) and the ionic radii of Nd^{III} and Ca^{II} are so close; they are 0.125 and 0.126 nm, respectively (20). It was partly successful and the compounds $Nd_{1-x}Ca_xCrO_4$ ($x = 0.02$–0.20) were synthesized as a single phase (by XRD and chemical analyses). Detailed crystal structures were determined by X-ray Rietveld method, and the mixed valence state of chromium and the vibrational modes of CrO_4 tetrahedra were investigated by X-ray photoelectron spectroscopy and Raman spectroscopy. The reason that the compounds with $x \geq 0.25$ were not obtained was discussed based on the geometrical change of CrO_4 tetrahedra.

EXPERIMENTAL

$NdCrO_4$ is synthesized by pyrolysis of the precursor at 853 K for 3 h in air: the precursor was prepared by vacuum drying of the equimolar solutions of $Nd(CH_3COO)_3$ and

0022-4596/01 $35.00

CrO_3 at 343 K, followed by preheating at 673 K in air, as reported previously (18). The same procedure was applied for synthesis of $Nd_{1-x}Ca_xCrO_{4-\delta}$. The precursors were prepared from stoichiometric solutions of $Nd(CH_3COO)_3$ (99.9% pure), $Ca(CH_3COO)_2$ (reagent grade), and CrO_3 (reagent grade), metal concentration being determined by chelatometry and redox titration. The mole ratio of neodimium to calcium, Nd/Ca, was changed in the range of 0.98/0.02–0.05/0.95. Pyrolysis conditions of the precursor to form single phase $Nd_{1-x}Ca_xCrO_{4-\delta}$ were investigated by thermo-gravimetry and differential thermal analysis (TG-DTA) and X-ray diffraction (XRD).

Chemical composition of $Nd_{1-x}Ca_xCrO_{4-\delta}$, prepared as a single phase, was determined by chemical analysis. About 0.5 g of a $Nd_{1-x}Ca_xCrO_{4-\delta}$ sample was dissolved in 100 cm^3 of 10 mol dm^{-3} H_2SO_4 solution. $Nd_{1-x}Ca_xCrO_{4-\delta}$ dissolves into a sulfuric acid solution by the disproportionation reaction of Cr^{V} ions as follows:

$$3Cr^{V} + 2Cr^{VI} + Cr^{III}. \qquad [1]$$

Concentration of Nd^{3+} and Ca^{2+} ions was determined by chelatometry with an EDTA solution, and that for CrO_4^{2-} anions by redox titration with an Fe^{II} solution. The density of the compounds was measured in CCl_4 using a liquid pycnometer.

X-ray diffraction patterns were measured by a JEOL rotating anode diffractometer with a monochromator under the following conditions: Cu$K\alpha$, 30 kV, 300 mA; scanning step, 0.02° (2θ); counting time, 20–25 s/step. The XRD data were collected in the 2θ range of 14° to 110°. Structure refinement by the Rietveld method was carried out using the RIETAN program (21). The peak shape was represented by a pseudo-Voigt function (22). Because the atomic scattering factor and dispersion correction for Cr^{V} were not found, these were assumed to be the same as those of the Cr atom (22).

Chemical states of chromium in $Nd_{1-x}Ca_xCrO_{4-\delta}$ were investigated by X-ray photoelectron spectroscopy (XPS) and Raman spectroscopy. Details of XPS measurement have been described elsewhere (23). Raman spectroscopic measurements were carried out by a triple-type monochromator (JASCO NRS-2000) under the irradiation of an argon ion laser (514.2 nm) of 30 mW. During the measurements, a sample, pressed in a disc shape of ca. 10 mm in diameter and 1 mm in thickness, was set on a stainless steel holder and rotated at 600 rpm to avoid the decomposition by the laser beam.

RESULTS AND DISCUSSION

Synthesis and Structure Refinement of $Nd_{1-x}Ca_xCrO_{4-\delta}$

Significant difference was not observed in the thermal decomposition behavior of the precursors with Nd/Ca = 0.98/0.02, 0.90/0.10, 0.85/0.15, and 0.80/0.20. There was an intermediate plateau in the region of 813–923 K in the TG curve and an endothermic peak appeared around 823 K in the DTA curve, under oxygen atmosphere. Based on the TG-DTA data, pyrolysis at constant temperatures around 823 K in O_2 was carried out to determine the condition to prepare single-phase compounds (by XRD). Consequently, the pyrolysis at 823–843 K for 6–12 days in O_2 were found to be the most suitable conditions under which synthesize the single phases of zircon type $Nd_{1-x}Ca_xCrO_{4-\delta}$ ($x = 0.02$–0.20). The polycrystalline samples thus prepared were well crystallized and all peaks of XRD patterns were indexed as a tetragonal zircon type.

In the TG curves for Nd/Ca = 0.75/0.25 and 0.70/0.30, a distinct plateau was not observed in the temperature range of 800–900 K at any partial oxygen pressure, P_{O_2}, from 0 to 1 atm, though weight decrease was observed. The XRD patterns of the pyrolysis products at constant temperatures of 800–900 K showed that the secondary phases of the perovskite-type oxides were formed. Above 900 K only perovskite-type compounds were formed. In the case of higher calcium content, Nd/Ca = 0.05/0.95, only the mixtures of $CaCrO_4$ and perovskite-type $Nd_{1-y}Ca_yCrO_3$ were obtained at any temperatures and under $0 \le P_{O_2} \le 1$. Therefore, it is reasonable to conclude that there is a threshold composition of Nd/Ca between 0.80/0.20 and 0.75/0.25 for forming $Nd_{1-x}Ca_xCrO_{4-\delta}$ (in other words, less than 25% of Nd^{III} can be replaced by Ca^{II}) and that substitution of Ca^{II} by Nd^{III} in $CaCrO_4$ may not be possible under $0 \le P_{O_2} \le 1$.

Chemical composition of $Nd_{1-x}Ca_xCrO_{4-\delta}$ prepared as a single phase is summarized in Table 1, indicating that the deviations from the initial proportion are very small and δ can be regarded as zero. Accordingly, these compounds have no nominal oxygen defects created by aliovalent substitution. The concentration of Cr^{VI} components resulted by the disproportional dissolution were in agreement with the expected value from the formula $Nd_{1-x}Ca_xCr^{V}_{1-x}Cr^{VI}_xO_4$ ($x = 0.02$–0.20). Above results suggest that the charge compensation is made by the presence of Cr^{VI}. It is favorable to the structure of zircon type $NdCrO_4$, where all oxygen atoms bond to chromium atoms to form the oxometallate, CrO_4^{3-} ions. Any oxygen defects in this structure may produce species like $CrO_3^{\bullet}$ which involve the dangling bonds. It is difficult to introduce systematically such unstable species into the crystal, since Cr–O bonds of CrO_4^{3-} tetrahedron in $NdCrO_4$ have strong covalency (18). Hereafter, all the plots as a function of x are based on the analyzed values in Table 1 and nominal values such as $x = 0.10$ are used for symbols.

The Rietveld structural refinement of $Nd_{1-x}Ca_xCrO_4$ ($x = 0.02$–0.20) was carried out in the zircon-type (space group $I4_1/amd$) model; the neodymium and calcium atoms occupy 4*a* (0, $\frac{3}{4}$, $\frac{1}{2}$), chromium atoms 4*b* (0, $\frac{1}{4}$, $\frac{3}{8}$), and oxygen

TABLE 1
Chemical Composition of $Nd_{1-x}Ca_xCrO_4$

x (nominal)	Composition (determined)	Averaged valence of Cr (observed)
0.02	$Nd_{0.981(2)}Ca_{0.025(2)}Cr_{1.00}O_{4.03(1)}$	5.07 +
0.10	$Nd_{0.893(1)}Ca_{0.094(2)}Cr_{1.00}O_{3.98(1)}$	5.09 +
0.15	$Nd_{0.844(1)}Ca_{0.156(1)}Cr_{1.00}O_{4.01(1)}$	5.18 +
0.20	$Nd_{0.792(2)}Ca_{0.208(2)}Cr_{1.00}O_{3.99(1)}$	5.19 +

atoms 16*h* (0, O_y, O_z). On refinement, the data for $NdVO_4$ was used as a starting model for the initial oxygen positions and thermal parameters, which were determined by neutron diffraction experiments (24), and isotropic thermal parameters B_{eq} were employed. The site occupancies for each site were fixed to the values from the chemical analyses. The final Rietveld profiles for $Nd_{1-x}Ca_xCrO_4$ ($x = 0.02$–0.20) are shown in Fig. 1. The refined crystallographic data together with reliability factors are given in Table 2. For all samples, the reliability factors (R_{wp}, R_p, R_F, and R_{exp}) are sufficiently small, and G of F factor (goodness of fitting indicator, R_{wp}/R_{exp}) is less than the required limit of 1.3, except for 1.33 of $x = 0.02$. The values in Table 2 indicate that the structural refinements converged well. Measured densities of $Nd_{1-x}Ca_xCrO_4$ ($x = 0.02$–0.20) are also listed in Table 2. They are in good agreement with the calculated ones. The results of Rietveld structure refinement confirm that $Nd_{1-x}Ca_xCrO_4$ ($x = 0.02$–0.10) is single phase of zircon-type oxide. The selected bond lengths and angles are listed in Table 3.

TABLE 2
Reliability Factors and Crystallographic Data, Refined by the Powder X-ray Rietveld Methods for $Nd_{1-x}Ca_xCrO_4$ ($x = 0.02$–0.20)

	$x = 0.02$	$x = 0.10$	$x = 0.15$	$x = 0.20$
R_{wp} (%)	13.73	10.01	11.25	10.12
R_p	9.66	8.52	9.23	8.78
R_I	2.98	2.81	2.96	2.91
R_F	2.21	1.88	2.12	1.92
G of F	1.33	1.26	1.22	1.27
a (nm)	0.73085(2)	0.73073(1)	0.73024(1)	0.72993(1)
c (nm)	0.63974(1)	0.63967(1)	0.63910(1)	0.63887(1)
O_y	0.4305(5)	0.4295(3)	0.4280(4)	0.4279(3)
O_z	0.2070(3)	0.2070(2)	0.2079(3)	0.2088(3)
B_{eq} (Nd and Ca) (Å^2)	0.36(3)	0.48(1)	0.38(2)	0.35(1)
B_{eq} (Cr)	0.42(3)	0.58(3)	0.61(2)	0.68(2)
B_{eq} (O)	0.54(2)	0.88(5)	0.75(5)	0.85(5)
D_x (calc.) (g cm^{-3})	5.0196	4.8581	4.7674	4.6715
D_x (obs.) (g cm^{-3})	5.022	4.859	4.770	4.673
No. of reflection	134	130	124	124
Color	Dark green	Green	Yellow green	Yellow green

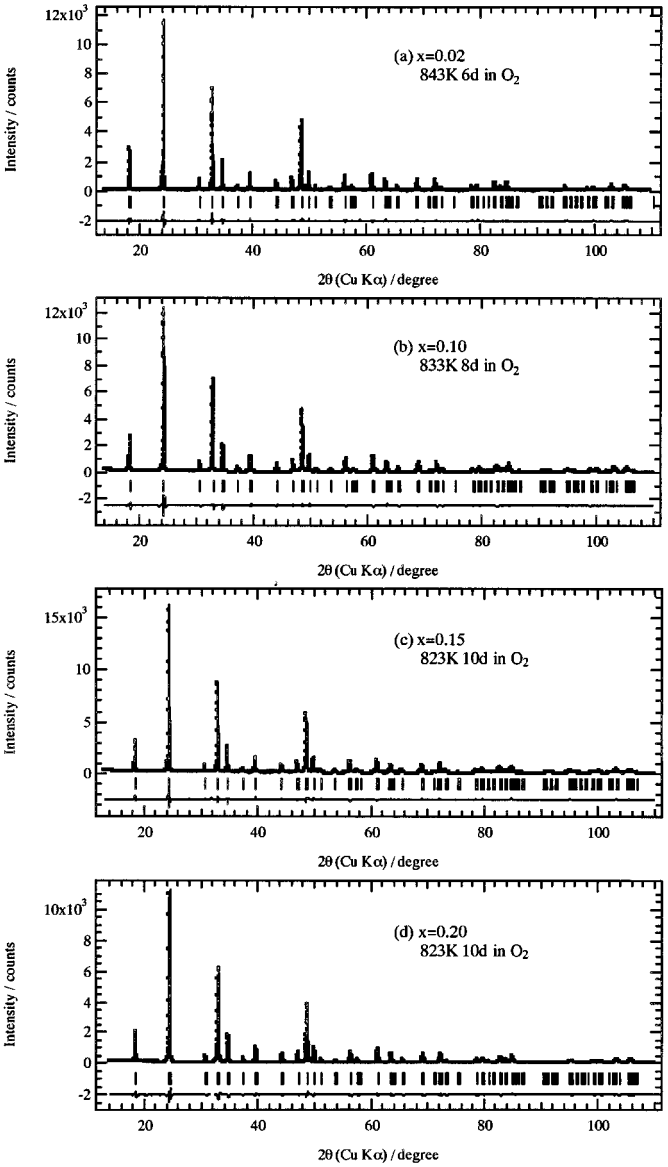

FIG. 1. Powder X-ray diffraction patterns of $Nd_{1-x}Ca_xCrO_4$, together with the final Rietveld refinement profiles, for $x =$ (a) 0.02, (b) 0.10, (c) 0.15, and (d) 0.20, respectively. Temperature and time indicate annealing conditions.

XPS and Raman Spectroscopic Analysis

The XPS spectra of Cr 2*p* for $Nd_{1-x}Ca_xCrO_4$ ($x = 0$, 0.10, and 0.20) are shown in Fig. 2. Previously, we reported that the binding energies, E_B, for $NdCrO_4$, are $E_B[Cr\ 2p_{3/2}] = 579.0$ eV and $E_B[Cr\ 2p_{1/2}] = 588.3$ eV (18), in good agreement with those for $LaCrO_4$, in which the formal valence of chromium is pentavalent (23). Cr $2p_{3/2}$ peak for $x = 0.10$ and 0.20 clearly indicates the appearance of an extra component having higher E_B than that for pentavalent chromium, and its intensity is increasing with x. $E_B[Cr\ 2p_{3/2}]$ of the peak maximum for $x = 0.20$ is about

TABLE 3
Selected Bond Lengths, Interatomic Distances, and Bond Angles in $Nd_{1-x}Ca_xCrO_4$ ($x = 0$–0.20)

	$x = 0.02$	$x = 0.10$	$x = 0.15$	$x = 0.20$
Bond length (nm)				
Cr–O (×4)	0.1701(4)	0.1696(2)	0.1682(2)	0.1677(2)
Short Nd–O (×4)	0.2393(7)	0.2400(6)	0.2410(6)	0.2412(5)
Long Nd–O (×4)	0.2500(6)	0.2496(4)	0.2493(6)	0.2497(4)
Angle (°)				
Small O–Cr–O (×2)	101.7	101.3	101.2	101.5
Large O–Cr–O (×4)	113.5	113.7	113.8	113.6
Distance (nm)				
Shortest O–O	0.2843(3)	0.2841(2)	0.2856(3)	0.2869(2)

580 eV and it coincides with that of hexavalent chromate (25). The changes in Cr $2p_{1/2}$ peak is a little ambiguous but still a small shoulder is observable at the higher E_B side and FWHM for $x = 0.10$ and 0.20 is broader than that of $x = 0$. Apparently, the peak height of Cr^{VI} for $x = 0.2$ is larger than Cr^{V} but this is due to the following reasons: (a) Cr^{VI} peak width is narrower than that of Cr^{V} peak, (b) Cr^{VI} peak is superposed on the tail of Cr^{V} peak, and (c) the information by XPS is confined to the very thin surface layer and Cr^{VI} species might segregate slightly on the surface: it may occur by pressing the sample to a holder. *M* 2*p* spectra for several of the first-low transitional metals have complicated structures which arise from a splitting of the *M* 2*p* lines due to a coupling, so that it is theoretically incorrect to describe each component by using a single asymmetric function (26), though many authors reported such results. Therefore, peak separation of Cr 2*p* spectra in Fig. 2 is practically impossible but the above evidences are sufficient to show that $Nd_{1-x}Ca_xCrO_4$ ($x = 0.10$ and 0.20) contain both pentavalent and hexavalent chromium ions.

Further evidence for the mixed valency was obtained by Raman spectroscopy, as shown in Figs. 3 and 4, where the spectra for $NdCrO_4$ ($Cr^{V}O_4^{3-}$ tetrahedron) and $CaCrO_4$ ($Cr^{VI}O_4^{2-}$ tetrahedron) are also shown for references. The zircon types $NdCrO_4$ and $CaCrO_4$ have the isolated tetrahedral CrO_4 oxometallates with D_{2d} symmetry. Based on the site group analysis, all Raman bands observed in 1000–150 cm^{-1} for $NdCrO_4$ and $CaCrO_4$ are assigned as an internal vibration to the vibrational modes of CrO_4 tetrahedra (18, 27). The site group analysis gives the internal vibrational modes of D_{2d} symmetric tetrahedron as ν_1 (the symmetric stretching modes of the A_1 symmetry), ν_2 (the symmetric bending modes of the $A_1 + B_1$ symmetry), ν_3 (the antisymmetric bending modes of the $B_2 + E$ symmetry), and ν_4 (the antisymmetric bending modes of the $B_2 + E$ symmetry). Hereafter, symbols with prime such as ν_1' and ν_2' refer to $Cr^{VI}O_4^{2-}$ tetrahedra. In $NdCrO_4$ one peak was observed

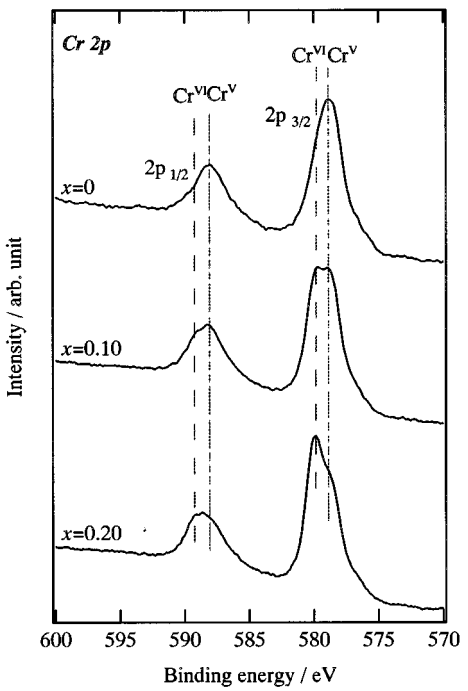

FIG. 2. XPS spectra of Cr 2*p* for $Nd_{1-x}Ca_xCrO_4$ ($x = 0$, 0.10, and 0.20).

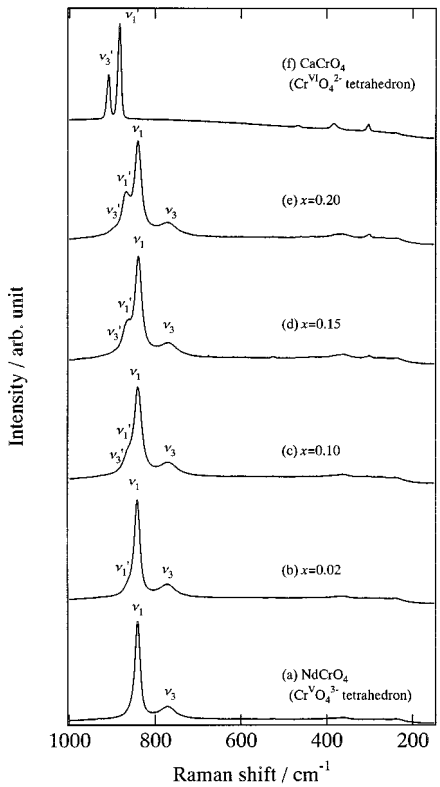

FIG. 3. Raman spectra of the stretching modes, ν_1 and ν_3, of $Cr^{V}O_4^{3-}$ and $Cr^{VI}O_4^{2-}$ units in Nd_{1-x}–Ca_xCrO_4, with $x =$ (a) 0, (b) 0.02, (c) 0.10, (d) 0.15, (e) 0.20, and (f) $CaCrO_4$. Primes on symbols were used only to distinguish the vibrational modes of $Cr^{VI}O_4^{2-}$ from those of $Cr^{V}O_4^{3-}$.

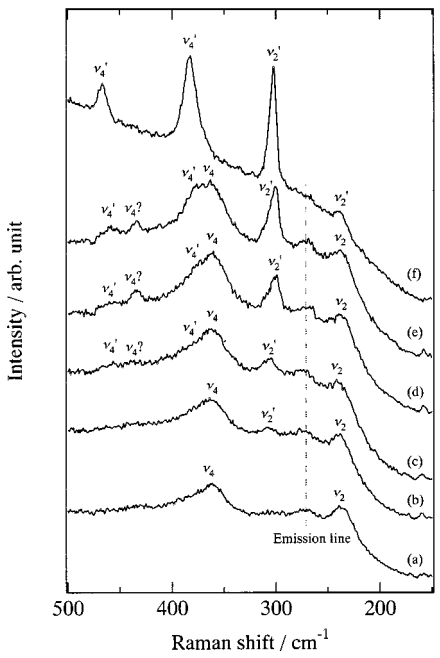

FIG. 4. Raman spectra of the weak vending modes, v_2 and v_4, of $Cr^{V}O_4^{3-}$ units in $Nd_{1-x}Ca_xCrO_4$, with x = (a) 0, (b) 0.02, (c) 0.10, (d) 0.15, (e) 0.20, and (f) $CaCrO_4$. Primes on symbols were used only to distinguish the vibrational modes of $Cr^{VI}O_4^{2-}$ from those of $Cr^{V}O_4^{3-}$.

for each vibrational mode of v_1 to v_4; that is, the degeneration of the vibrational modes did not split apparently (18), whereas that of v'_2 and v'_4 modes splits in $CaCrO_4$ (27). The observed Raman bands are distributed in two well-separated wave number regions, corresponding to the Cr–O stretching modes (920–700 cm^{-1}) and O–Cr–O bending modes (200–400 cm^{-1}). The assignment of Raman bands for both compounds is summarized in Table 4. Though the v' values and assignment for $CaCrO_4$ in Ref. 27 were based on the infrared absorption spectroscopy, they were used for references.

Based on the assignment to above two terminal compounds, Raman spectra of $Nd_{1-x}Ca_xCrO_4$ series were identified as shown in Figs. 3 and 4 and Table 4. It is clearly seen with increasing x that the spectra of Cr–O stretching modes for $Cr^{VI}O_4^{2-}$, v'_1 and v'_3 peaks, are superimposed on those for $Cr^{V}O_4^{3-}$, v_1 and v_3 peaks, and that the relative intensities for $Cr^{VI}O_4^{2-}$ are increasing. The spectra of O–Cr–O bending modes were weak but all vibrational modes were reasonably assigned, since they were well separated. Very weak v'_2 bands emerged around 300 cm^{-1} for $x = 0.02$ and grew up with increasing x. A very weak v'_4 band started to appear around 455 cm^{-1} from $x = 0.10$. Another v'_4 band was distinguishable as a shoulder on the high wave number side of v_4 band above $x = 0.10$; however, v'_2 of the lowest wave number was undistinguishable due to the overlap of v_2 band. In $x = 0.10$–0.20, an additional peak appeared around 435 cm^{-1}, which was not observed in $NdCrO_4$. The peak is indicated as v_4? in Fig. 4, since it cannot be an additional v'_4 band. Tentatively, this assignment is the most probable by considering the structural changes of CrO_4 tetrahedra with x, as discussed later. At all the peak intensities for $Cr^{IV}O_4^{2-}$ are increasing with increasing x in $Nd_{1-x}Ca_xCrO_4$, two types of tetrahedra, $Cr^{V}O_4^{3-}$ and $Cr^{VI}O_4^{2-}$, are coexistent in these compounds. Therefore, it is concluded that the imbalance created by aliovalent substitution is compensated by the presence of $Cr^{VI}O_4^{2-}$, though

TABLE 4
The Observed Peak Positions (cm^{-1}) and Assignment of Raman spectra in $Nd_{1-x}Ca_xCrO_4$ (x = 0–0.20) and $CaCrO_4$

	Assignment and peak position							
	$Cr^{V}O_4^{3-}$ tetrahedra				$Cr^{VI}O_4^{2-}$ tetrahedra			
	v_1	v_2	v_3	v_4	v'_1	v'_2	v'_3	v'_4
$NdCrO_4$ ($x = 0$)	844.0 (ss)	240.3 (vw)	775.8 (bs)	363.9 (vw)				
$x = 0.02$	840.8 (ss)	237.7 (vw)	768.4 (bs)	361.1 (vw)	858.4 (wsh)	302.6 (vw)		
$x = 0.10$	839.8 (ss)	236.7 (vw)	766.5 (bs)	361.1 (vw) 436.2 (bvw)[a]	862.1 (sh)	303.5 (vw)	900.1 (wsh)	373.1 (wsh) 455.7 (bvw)
$x = 0.15$	839.2 (ss)	237.1 (vw)	766.9 (bs)	360.5 (w) 435.6 (vw)[a]	861.5 (sh)	299.2 (vw)	895.8 (wsh)	372.5 (wsh) 457.9 (bvw)
$x = 0.20$	840.2 (ss)	238.0 (vw)	767.8 (bs)	363.2 (w) 433.8 (vw)	868.9 (s)	301.1 (w)	897.7 (wsh)	378.1 (wsh) 458.8 (vw)
$CaCrO_4$					882.8 (ss)	302.9 (w) 204.5 (vw)	908.8 (ss) 925[b] 892[b]	382.7 (w) 467.2 (vw) 411[b]

[a]Tentatively assigned to v_4.
[b]IR data cited from Ref. 27.

the creation of the trace amounts of oxygen vacancies cannot be eliminated. The $Nd_{1-x}Ca_xCrO_4$ ($x = 0.02$–0.20) compounds are categorized to the CLASS II mixed valence oxides described by Day and Robin (28).

Structural Analysis and Stability of $Nd_{1-x}Ca_xCrO_4$

As $Nd_{1-x}Ca_xCrO_4$ ($x = 0.02$–0.20) are composed of $Cr^{V}O_4^{3-}$ and $Cr^{VI}O_4^{2-}$, lattice constants a and c change with x. As shown in Fig. 5, both decrease linearly with increasing x in the range of $x = 0$–0.20 (Fig. 5b) but the relation deviates from the Vegard's law between $NdCrO_4$ and $CaCrO_4$ (Fig. 5a). Here the data for the terminal compounds were cited from the previous work (18) and Ref. 19. These changes are reflected to the atomic position of 16*h* oxygen as shown in Fig. 6, where, *X*-coordinate, O_x, was taken to be 0.0000. *Y*-coordinate, O_y, generally decreases with x and marked decrease is observed between $x = 0.10$ and $x = 0.15$. *Z*-coordinate, O_z, is nearly constant up to $x = 0.10$ and increases linearly beyond it. O_z for the terminal compound $CaCrO_4$ is 0.2070 and almost the same with that for the other terminal compound $NdCrO_4$.

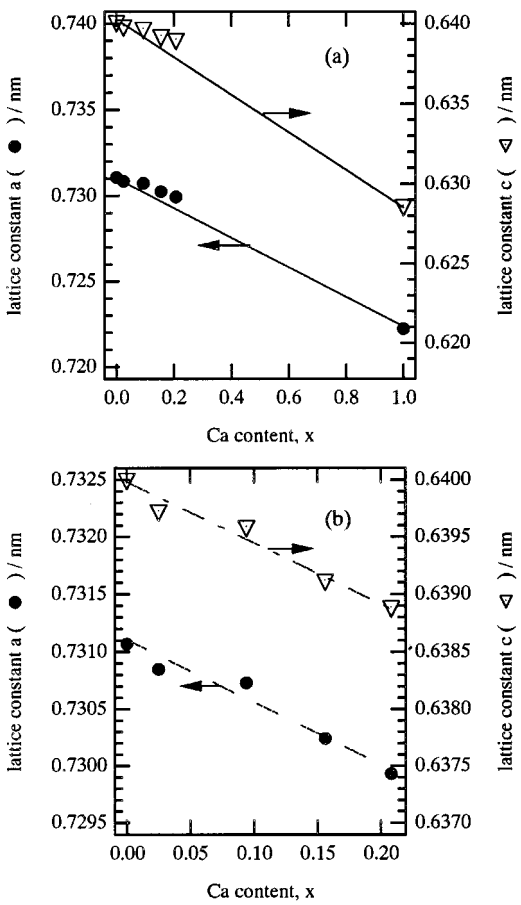

FIG. 5. Change of the lattice constants a (●) and c (▽) with x in $Nd_{1-x}Ca_xCrO_4$ in the ranges of (a) 0–1.00 and (b) 0–0.20.

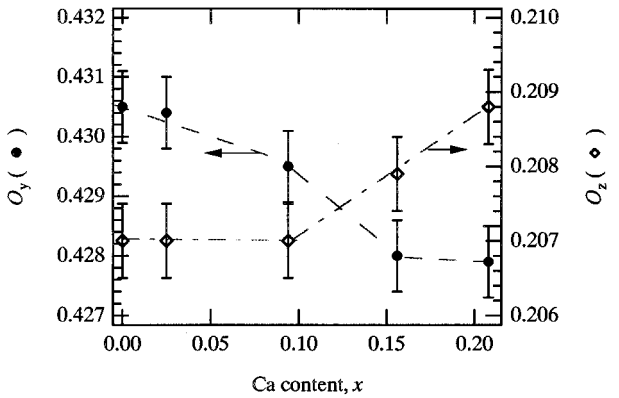

FIG. 6. Change of 16*h* oxygen position in $Nd_{1-x}Ca_xCrO_4$, with x: O_y (●) and O_z (◇).

Accordingly, O_z value for $x = 0.15$ and 0.20 is exceptionally larger than for others. It should be noted here that the date described in this section are based on the XRD measurements, so that the effects caused by the coexistence of $Cr^{V}O_4^{3-}$ and $Cr^{VI}O_4^{2-}$ are averaged because only a single zircon-type phase is observed by XRD.

The above results suggest that the shape of CrO_4 tetrahedra in $Nd_{1-x}Ca_xCrO_4$ changes discontinuously with increasing x. Figure 7a indicates the 200 plane of zircon type $NdCrO_4$. This plane reflects a feature of zircon-type structure and can be projected onto an equivalent 040 plane by symmetric operations of the space group, as shown in Fig. 7b. Naturally, $Nd_{1-x}Ca_xCrO_4$ and $CaCrO_4$ have the same characteristic planes. The changes of O_y and O_z shown in Fig. 6 cause displacement of oxygen along *b*- and *c*-axes as shown by arrows in Fig. 7c. Consequently, the average Cr–O bond length is expected to decrease in $Nd_{1-x}Ca_xCrO_4$, especially in $x = 0.15$ and 0.20. Variation of Cr–O bond length with x is shown in Figs. 8a1 and 8a2. As CrO_4 tetrahedron of D_{2d} symmetry has four Cr–O bonds of the same length, the average bond length for the mixture of $Cr^{V}O_4^{3-}$ and $Cr^{VI}O_4^{2-}$ tetrahedra, L_{calc}, is simply calculated by

$$L_{calc} = (1 - x)L_{Cr(V)-O} + xL_{Cr(VI)-O}, \qquad [2]$$

where $L_{Cr(V)-O}$ and $L_{Cr(VI)-O}$ are the bond lengths of Cr–O in $NdCrO_4$ and $CaCrO_4$, 0.1702 nm (18) and 0.1647 nm (19) respectively. A solid straight line in Fig. 8a1 is the result of calculation. Except for $x = 0.15$ and 0.20, the observed Cr–O bond lengths lie on this line from $NdCrO_4$ through $x = 0.02$ and 0.10 to $CaCrO_4$. It is seen from the plotting for $x = 0$–0.20 (Fig. 8a2) that the change is in parallel with the results in Fig. 6. In Figs. 8a1 and 8a2, the shortest O–O distance between neighboring CrO_4 units, which is schematically shown in Fig. 7c, is also plotted against x. Again the values for $x = 0.15$ and 0.20 deviate from a trend. The change of this O–O distance with x resembles that of O_z in

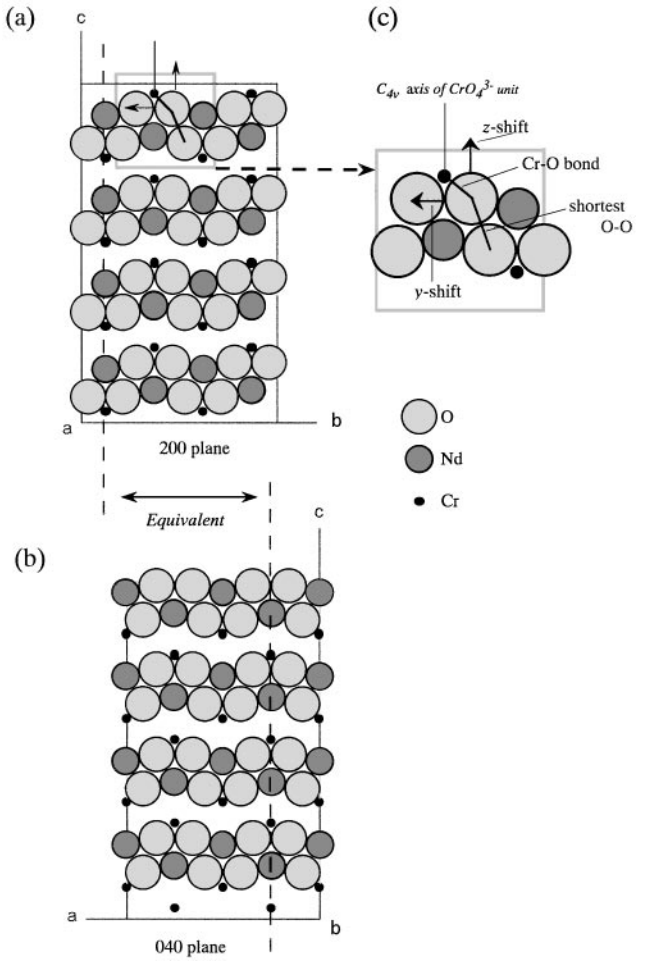

FIG. 7. (a) 200 and (b) 040 planes of zircon type $NdCrO_4$, and (c) the magnified area indicated by the gray square in (a). In (a) and (b), Cr and Nd atoms on the vertical broken lines are located in both planes.

Fig. 6, indicating that the O_z shift influences the distance more sensitively than the O_y shift. The D_{2d} symmetry CrO_4 tetrahedron has two kinds of O–Cr–O bond angles, so that they were plotted as a function of x in Figs. 8b1 and 8b2 to visualize the deformation of CrO_4 tetrahedra more clearly. Unexpectedly, the smaller angle decreased and the larger angle increased with increasing x from 0 to 0.15. This indicates that CrO_4 tetrahedra are elongating up to $x = 0.15$. If $Cr^{V}O_4^{3-}$ and $Cr^{VI}O_4^{2-}$ simply coexist in the structure, both angles should approach monotonously to the values of $Cr^{VI}O_4^{2-}$ with increasing x, since they are the averages of those in $Cr^{V}O_4^{3-}$ and $Cr^{VI}O_4^{2-}$. Above $x = 0.15$, this tendency reverses and the values direct toward those of $Cr^{VI}O_4^{2-}$, but the smaller angles for $x = 0.20$ are still smaller than those of $NdCrO_4$ and the larger ones are still larger. It is estimated from Figs. 8b1 and 8b2 that the both angles cross the values of $NdCrO_4$ at around $x = 0.25$. As mentioned above (Fig. 4 and Table 4), a new peak appeared in the Raman spectra of $x = 0.10$–0.20 around 435 cm^{-1}, and it was tentatively assigned to an additional v_4 band. The splitting of degeneration may be possible by the elongation of $Cr^{V}O_4^{3-}$ tetrahedra which results in the appearance of an additional v_4 band. It is probable that the v_2 band also splits but it is too weak to distinguish.

Above all the results suggest that there is a possibility of some interaction between $Cr^{V}O_4^{3-}$ and $Cr^{VI}O_4^{2-}$ when x is smaller than about 0.2. It might be a hint why the compound with $x \geq 0.25$ was never synthesized. Qualitatively, it may be possible to consider that a small amount of $Cr^{VI}O_4^{2-}$ tetrahedra which are less elongated and less charged than $Cr^{V}O_4^{3-}$ tetrahedra increase the shortest O–O distance (Fig. 8a) and reduce the coulomb repulsion between tetrahedra, but the large amounts deform the basic structure of $NdCrO_4$. It should be noted here that the shortest O–O distance in $NdCrO_4$ is shorter than that in $CaCrO_4$ (Fig. 8a1) but the lattice constants of the former are longer than those of the later (Fig. 5a). This is partly due to the difference in cations but the geometry of tetrahedra is a more important factor, since ionic radii of both cations are very close in the zircon-type structure.

It is worthwhile to add that the bond angles between $NdCrO_4$ and $x = 0.02$ are different on the calculation level; for example, the smaller angles were 101.69° and 101.66°, respectively. The final digit, however, is not so accurate that both were taken to be 101.7° in the figures. Atanasov reported by theoretical calculations for a $Cr^{V}O_4^{3-}$ tetrahedron terminated with protons that the tetrahedron was the most stable with 103.5° for the smaller angles in the ground states (29) (T_d symmetric tetrahedron has 109.45°) but it cannot be compared simply with our results.

CONCLUSIONS

Single-phase $Nd_{1-x}Ca_xCrO_4$ ($x = 0$–0.20) oxides were synthesized by the pyrolysis of precursors prepared from Nd^{III}–Ca^{II}–Cr^{VI} mixed solutions and the following structural features were found.

(i) All $Nd_{1-x}Ca_xCrO_4$ were zircon type (tetragonal, $I4_1/amd$), and the composition determined by chemical analyses did not differ from that of preparation, indicating that the compounds are almost stoichiometric without any essential defects.

(ii) XPS and Raman spectra indicated that $Nd_{1-x}Ca_xCrO_4$ ($x = 0.02$–0.20) are mixed valence oxides containing two types of tetrahedra, $Cr^{V}O_4^{3-}$ and $Cr^{VI}O_4^{2-}$, having D_{2d} symmetry in the structure, and this compensates for the decrease of positive charges introduced by Ca^{II} ions.

(iii) The lattice constants and atomic positions were refined by the X-ray Rietveld method. The calculated densities of $Nd_{1-x}Ca_xCrO_4$ ($x = 0$–0.20) were in good agreement with the ones measured by the picnometry. Though two types of tetrahedra were not distinguishable by XRD, lattice constants, a and c decreased almost linearly with x. The

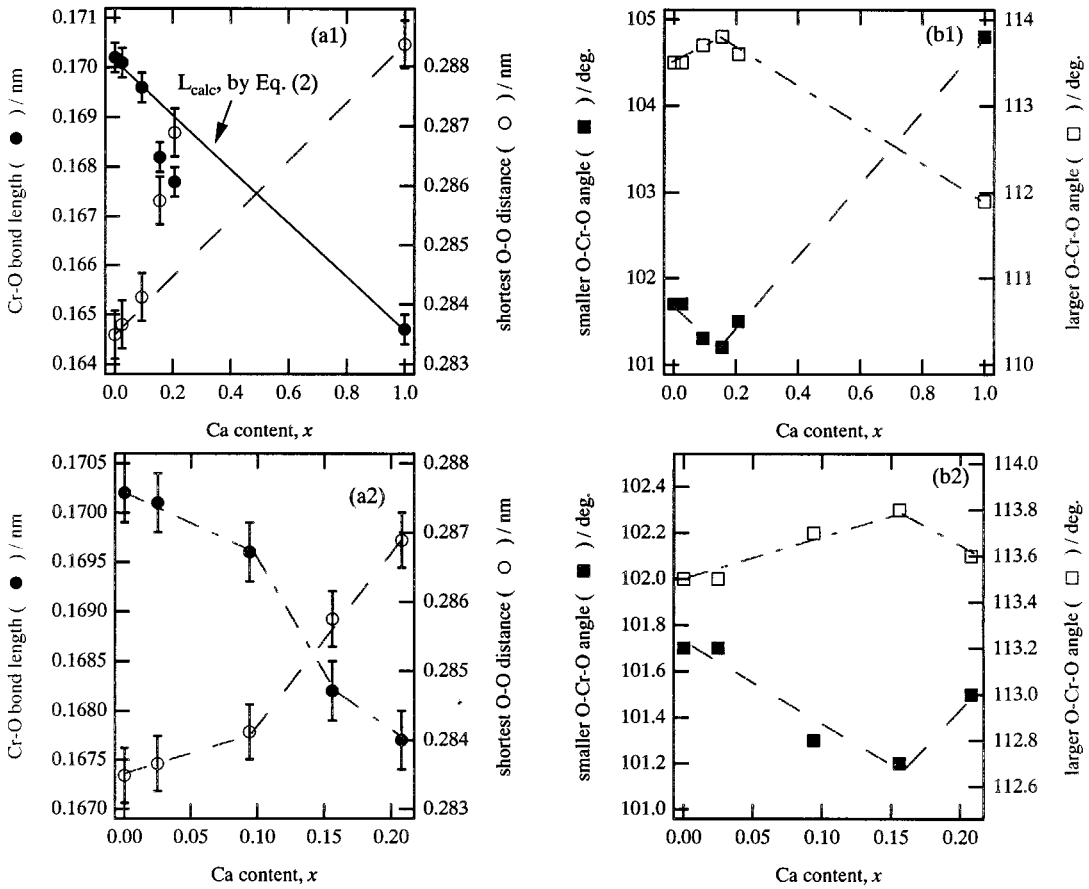

FIG. 8. Change of (a) the Cr–O bond length (●) and the shortest O–O distance (○), and (b) the smaller (■) and larger (□) O–Cr–O angles in $Nd_{1-x}Ca_xCrO_4$, with Ca content, x, in the range of (a1), (b1) 0–1.00 and (a2), (b2) 0–0.20. The solid line in (a1) shows the Cr–O bond length, calculated by Eq. [2].

values for $x = 0.02$–0.20, however, were not on the line expected by Vegard's law between $NdCrO_4$ and $CaCrO_4$ but larger.

(iv) The calculated O–Cr–O bond angles did not change monotonously as lattice constants and other crystallographic parameters such as Cr–O bond length did. The results indicated that CrO_4 tetrahedra in $Nd_{1-x}Ca_xCrO_4$ ($x = 0.02$–0.20) are more elongated (in average) than in $NdCrO_4$ and $CaCrO_4$, and above $x =$ ca.0.25 the tetrahedra become less elongated and approach to the shape of $Cr^{VI}O_4^{2-}$ tetrahedra with increasing x.

(v) It was deduced that a small amount of $Cr^{VI}O_4^{2-}$ tetrahedra which are less elongated and less charged than $Cr^{V}O_4^{3-}$ tetrahedra reduce the coulomb repulsion between tetrahedra, but the large amounts deform the basic structure of $NdCrO_4$.

REFERENCES

1. C. Albrecht, S. Cohen, I. Mayer, and D. Reinen, *J. Solid State Chem.* **107,** 218 (1993).
2. T. C. Brunold, M. F. Hazenkamp, and H. U. Gudel, *J. Am. Chem. Soc.* **107,** 5598 (1995).
3. T. C. Brinold and H. U. Gudel, *Chem. Phys. Lett.* **249,** 77 (1996).
4. T. Ziegler, A. Rauk, and E. J. Baerends, *Chem. Phys.* **16,** 209 (1976).
5. M. F. Hazenkamp and H. U. Gudel, *Chem. Phys. Lett.* **251,** 310 (1996).
6. M. Atanasov, H. Adamsky, and K. Eifert, *J. Solid State Chem.* **128,** 1 (1997).
7. M. Atanasov, *Chem. Phys.* **195,** 49 (1995).
8. H. Schwarz, *Z. Anorg. Allge. Chem.* **322,** 1 (1963).
9. H. Schwarz, *Z. Anorg. Allge. Chem.* **322,** 15 (1963).
10. H. Schwarz, *Z. Anorg. Allge. Chem.* **322,** 129 (1963).
11. H. Schwarz, *Z. Anorg. Allge. Chem.* **323,** 275 (1963).
12. H. Walter, H. G. Kahle, K. Mulder, H. C. Schopper, and H. Schwarz, *Int. J. Magn.* **5,** 129 (1973).
13. G. Buisson, F. Tcheou, F. Sayetat, and K. Scheuemann, *Solid State Commun.* **18,** 871 (1976).
14. A. Roy and K. Nag, *J. Inorg. Nucl. Chem.* **40,** 1501 (1978).
15. M. Steiner, H. Dachs, and H. Ott, *Solid State Commun.* **29,** 231 (1979).
16. S. G. Manca and E. J. Baran, *J. Phys. Chem. Solid.* **42,** 923 (1981).
17. A. Morales-Sanchez, F. Fernandez, and R. Saez-Puche, *J. Alloy. Compd.* **201,** 161 (1993).
18. Y. Aoki, H, Konno, H. Tachikawa, and M. Inagaki, *Bull. Chem. Soc. Jpn.* **73,** 1197 (2000).
19. G. Weber and K.-J. Range, *Z. Naturforsch.* **51**b, 751 (1996).
20. R. D. Shannon, *Acta Crystallogr. A* **32,** 751 (1976).

21. F. Izumi, H. Asano, H. Murata, and N. Watanabe, *J. Appl. Crystallogr.* **20,** 411 (1987).
22. "The Rietveld Method" (R. A. Young, Ed.), pp. 43–197. IUCr/OUP, Oxford, 1993.
23. H. Konno, H. Tachikawa, A. Furusaki, and R. Furuichi, *Anal. Sci.* **8,** 641 (1992).
24. B. C. Chakoumakos, M. M. Abraham, and L. A. Boatner, *J. Solid State Chem.* **109,** 197 (1994).
25. C. D. Wagner, "Practical Surface Analysis," 2nd ed., p. 595. Wiley, New York, 1990.
26. A. R. Pratt and N. S. McIntyre, *Surf. Interface Anal.* **24,** 529 (1996).
27. A. Muller, E. J. Baran, and R. O. Carer, *Struct. Bonding* **26,** 81 (1976).
28. P. Day, *Int. Rev. Phys. Chem.* **1,** 149 (1981).
29. M. Atanasov, *Z. Phys. Chem.* **200,** 57 (1997).